Heliyon 9 (2023) e12515

Contents lists available at ScienceDirect

Heliyon

journal homepage: www.cell.com/heliyon

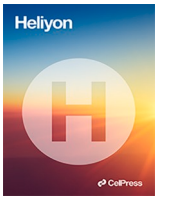

Research article

Metabolomic analysis of circulating tumor cells derived liver metastasis of colorectal cancer

Meng Li [a], Shengming Wu [b], Chengle Zhuang [a], Chenzhang Shi [a], Lei Gu [a], Peng Wang [b], Fangfang Guo [b], Yilong Wang [b,**], Zhongchen Liu [a,*]

[a] Department of General Surgery, Shanghai Tenth People's Hospital, School of Medicine, Tongji University, Shanghai 200092, PR China
[b] The Institute for Translational Nanomedicine, Shanghai East Hospital, The Institute for Biomedical Engineering & Nano Science, School of Medicine, Tongji University, Shanghai 200092, PR China

ARTICLE INFO

Keywords:
Circulating tumor cell
Metabolomics
Colorectal cancer
Liver metastasis
Mouse models

ABSTRACT

Metabolic reprogramming is one of the essential features of tumor that may dramatically contribute to metastasis and collapse. The metabolic profiling is investigated on the patient derived tissue and cancer cell line derived mouse metastasis xenograft. As well-recognized "seeds" for remote metastasis of tumor, role of circulating tumor cells (CTCs) in the study of metabolic reprogramming feature of tumor is yet to be elucidated. More specifically, whether there is difference of metabolic features of liver metastasis in colorectal cancer (CRC) derived from either CTCs or cancer cell line is still unknown. In this study, comprehensive untargeted metabolomics was performed using high performance liquid chromatography-mass spectrometry (HPLC-MS) in liver metastasis tissues from CT26 cells and CTCs derived mouse models. We identified 288 differential metabolites associated with the pathways such as one carbon pool by folate, folate biosynthesis and histidine metabolism through bioinformation analysis. Multiple gene expression was upregulated in the CTCs derived liver metastasis, specifically some specific enzymes. These results indicated that the metabolite phenotype and corresponding gene expression in the CTCs derived liver metastasis tissues was different from the parental CT26 cells, displaying a specific up-regulation of mRNAs involved in the above metabolism-related pathways. The metabolic profile of CTCs was characterized on the liver metastatic process in colorectal cancer. The invasion ability and chemo drug tolerance of the CTCs derived tumor and metastasis was found to be overwhelming higher than cell line derived counterpart. Identification of the differential metabolites will lead to a better understanding of the hallmarks of the cancer progression and metastasis, which may suggest potential attractive target for treating metastatic CRC.

1. Introduction

Colorectal cancer (CRC) is one of the most common malignant tumors in the world. Most CRC patients finally die owning to recurrence or tumor metastasis after routine treatment, particularly liver metastasis [1, 2]. Metabolic reprogramming is one of the essential characteristics of tumor cells, dominating cellular survival and maintenance, which have complicated effects on cancer

* Corresponding author.
** Corresponding author.
E-mail addresses: yilongwang@tongji.edu.cn (Y. Wang), lzc10th@tongji.edu.cn (Z. Liu).

https://doi.org/10.1016/j.heliyon.2022.e12515
Received 4 April 2022; Received in revised form 17 August 2022; Accepted 13 December 2022
Available online 21 December 2022

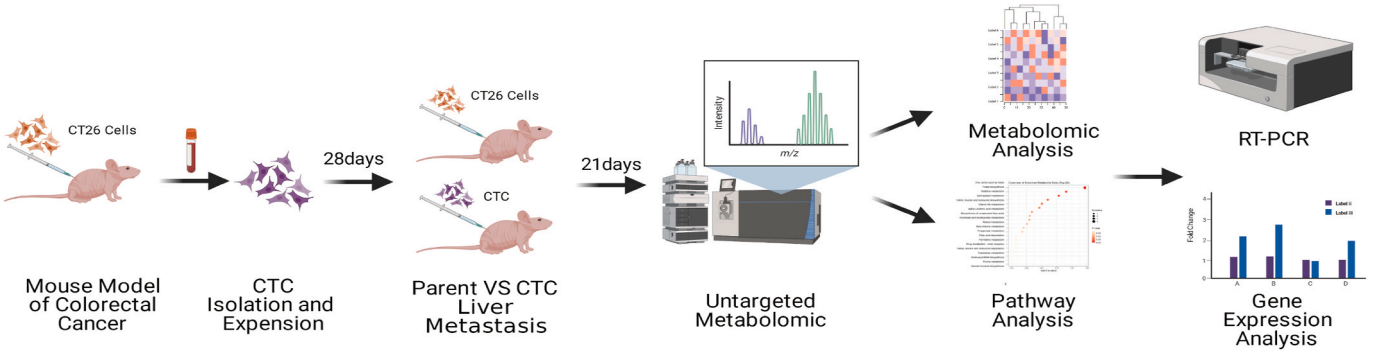

Figure 1. Flowchart of the experimental set-up.

metastasis [3, 4]. Circulating tumor cells (CTC) that shed from the primary tumor and intravasate into peripheral circulation system are recognized as tumor metastasis-initiating cells of several cancers, including the colorectal cancer, which has been shown as a valuable research target for tumor liquid biopsy and recapitulating the mechanism of cancer metastasis or recurrence [5, 6]. CTC-derived metastasis model is a powerful tool in the research of metabolic reprogramming related metastasis mechanisms and co-clinical research [7, 8].

However, the rarity and heterogeneity of the CTCs are great challenges for investigation of the metabolic feature. Evidence has emerged that CTCs are phenotypically heterogeneous, with certain CTC subgroups possessing higher metastatic potential [9, 10]. During the initiation of metastasis, tumor cells from primary tumors acquire an invasive or metastatic phenotype through epithelial-mesenchymal transition (EMT) and enter the circulation [11, 12]. Most CTCs die in the circulation due to a combination of physiologically environmental and mechanical factors; only a very small proportion of CTCs appears capable of survival and contributing to the metastasis [13]. So far, some significant progresses have been made to develop mouse models upon the isolated and *in-vitro* cultured CTCs. A recent study upon the CTC derived animal models have provided some conclusive remarks on the effect of CTC-neutrophil interaction on the metastasis and screening of the potential therapeutic target to suppress the spread of cancer [14, 15]. Metabolomic profiling of CTCs has been realized based on the liquid chromatography-mass spectrometry (LC-MS) [8]. This progress contributes to the investigation of the metabolic features of the CTC derived CRC liver metastasis.

So far, the feature of metabolic reprogramming of the liver metastasis derived from *in-vitro* cultivated CTC has not been fully elucidated. In this study, we compared the different metabolic features of liver metastasis of the CRC mouse derived from CT26 cells or *in-vitro* cultured CTCs by using high performance liquid chromatography-mass spectrometry (HPLC-MS) analysis. A set of metabolites and corresponding signaling pathways were identified, followed with the expression analysis of key molecules by RT-PCR. The workflow of this study is showed in Figure 1. Exploring the metabolic hallmark of the cancer progression and metastasis may provide potential attractive target for treating metastatic CRC.

2. Materials and methods

2.1. Cell culture

CT26 (CSTR:19375.09.3101MOUTCM37) cells bought from Chinese Academy of Sciences cell Bank were cultured in McCoy's 5A medium (Sangon Biotech, CN) supplemented with 10% FBS (MRC Inc., USA) and 1% Penicillin-Streptomycin Solution (Beyotime, CN). All cells were kept at 37 °C and 5% CO_2.

2.2. Mouse model

A total of 10 BALB/c nude mice (female, 4–6 weeks old, Shanghai Slake Laboratory Animal) were used for subcutaneous tumor formation experiment. The CT26 single-cell suspensions were suspended with Hank's balanced salt solution (HBSS) (Beyotime, CN). 2×10^6 cells were subcutaneously injected into the flank of each BALB/c nude mice. At the experiment's endpoint, the mice were terminated by cervical dislocation and blood was directly collected in EDTA tube by cardiac puncture.

A total of 12 BALB/c nude mice (female, 4–6 weeks old, Shanghai Slake Laboratory Animal) were used for mouse liver metastasis model. Mice were anaesthetized with inhalational anesthesia using 3% isoflurane for induction and 1.5% isoflurane for maintenance. Mice were randomly divided into two groups and with 6 mice/group: NC group (CT26 cells injected), E group (CTCs injected). An incision of around 1 cm was created on the abdominal cavity's left side. The spleen was softly separated, and 2×10^6 CT26 cells or CTCs were suspended in HBSS and injected into the lower pole of the spleen in 2 min. The spleen was returned to the abdominal cavity softly, and the cut was sutured and disinfected. After 21 days, the mice were sacrificed for liver collection.

2.3. CTC detection and immunocytochemical analyses

Red blood cells in blood sample were removed using erythrocyte lysis buffer (Beyotime, CN). Viable CTCs were negatively selected applying anti-CD45 antibody conjugated microbeads (Beaver Beads, CN) and magnetic rack following protocol of manufacturer. Then fixed with 4% Paraformaldehyde Fix Solution (Beyotime, CN) and made into cell smears. The sections were blocked for 30 min and incubated at 4 °C with CK, E-cad, CD44, CD45, Vimentin and Ki-67 antibodies (1:200, AbCam, USA) over-night. After incubating at 37 °C for 0.5 h and washing with PBS (5 min, 3 times), Alexa fluorescent secondary antibodies (1:500, Thermo Fisher, USA) and DAPI were added and stained at 37 °C in the dark for 1 h. They were observed and photographed under a confocal fluorescence microscope (TCS SP8 X, Leica). CTCs in the present study were defined as follows: DAPI+/CD45−/CK+.

2.4. Enrichment and ex vivo CTC culture

Erythrocyte lysis buffer was firstly used to eliminate red blood cells from blood sample. Viable CTCs were negatively selected applying CD45 microbeads and magnetic rack following protocol of manufacturer. Isolated CTCs were incubated at 5% CO^2 and 37 °C in 12 well non-adherent plates in McCoy's 5A medium that was supplemented with 1% Penicillin-Streptomycin Solution and 10% FBS. Single colonies from the CD45(−) population showed up during the second week of cell culture. They were transferred into 12-well plates for further growth and then into T25 flasks for culture expansion.

2.5. Migration and invasion assays

Cell migration assays was performed using 24-well modified Boyden chambers containing membrane filter (8 μm pores, BD, USA). The inserts were precoated with Matrigel (BD, USA). for the invasion assay. The lower chamber was filled with McCoy's 5A medium containing 10% FBS, whereas 1×10^4 CT26 cells or CTCs were placed in the upper part of chamber without FBS. The plates were incubated at 37 °C in 5% CO_2. Migration was quantified after 24 h, the cells that had migrated to the underside of the membrane was fixed with 4% paraformaldehyde and stained with 0.1% crystal violet. Photos were captured with a fluorescence microscope (ECLIPSE Ti, Nikon). Cells were counted under 200x magnified field, five randomly selected fields were counted for each condition and quantified using the ImageJ software. Invasion was quantified after 72 h, the other steps for cell invasion is similar to that of migration.

2.6. Histopathological analyses of the liver metastasis tissue

Mice liver metastasis tissues were fixed, paraffin-embedded, and sectioned in 3 μm sections. Tissue sections were first deparaffinized and rehydrated in xylene and serial alcohol solutions, respectively, and then stained with Hematoxylin-Eosin (HE). Images of tumor sections were acquired on a microscope (Eclipse E100, Nikon). Histological features and pathological diagnosis were made by a certified pathologist. The percentage of tumor cells were calculated under 40x magnified field, five randomly selected fields were calculated for each sections and quantified using the ImageJ software.

2.7. HPLC-MS

HPLC: 100 μL of each sample was separated on a Welch 2.1 × 150 mm RP-C18 column using a linear gradient in 30 min. The mobile phase consisted of 0.1% formic acid (Thermo Fisher, USA) in water (solvent A) and 0.1% formic acid in acetonitrile (Thermo Fisher, USA) (solvent B). The column was heated to 35 °C during analysis and flow rate was 0.3 mL/min. The gradient elution was in the following sequence: 0.0 min, 2%B; 1.0 min, 2%B; 5.0 min, 20%B; 10.0 min, 50%B; 15.0 min, 80%B; 20.0 min, 95%B; 25.0 min, 95%B; 26.0 min, 2%B; 30.0 min, 2%B.

MS: All data were acquired using a Q Exactive mass spectrometer operated in positive/negative polarity mode. The electrospray ionization (ESI) source was operated under the following conditions: Capillary temperature was at 300 °C and sheath gas flow rate was at 35 arb. Both positive and negative ions were scanned in a mode of fast switching between positive and negative ions at 3.8 kV spray voltage.

Data were collected from 100 to 1500 m/z using full MS-data dependent MS2 (ddMS2) scan mode at resolution 70,000 full width half maximum (FWHM) and 17,500 FWHM for full MS and MS2, respectively.

All MS2 spectra of the compounds were acquired at three fixed collision energies, 10, 30 and 45. The MS/MS spectra of metabolites were obtained by HPLC-MS/MS.

Data Processing: The acquired data from HPLC-MS analysis were sorted out by CD2.1 (Thermo Fisher Technology) and identified metabolites were realized by the database (mzCloud, mzVault). Data pretreatment procedures including peak detection, deconvolution, normalization, alignment, denoising, and data reduction. The parameters for peak detection: centWave m/z 25 ppm, peak width c (10, 60), prefilter c (10, 100); and parameters for chromatogram alignment, including mzwid = 0.025, minfrac = 0.5, and bw = 5. After being recognized and aligned, the intensity of each ion was normalized to the summed total ion intensity of each chromatogram. Only compounds with a high mzCloud match (>80) were assigned an identity and used in subsequent analyses. The processed data were performed using the OmicShare tools (https://www.omicshare.com/tools), including Univariate (volcano plots), multivariate [Principal component analysis (PCA), orthogonal partial least-squares discriminant analysis (OPLS-DA)], and cluster (heatmap) analyses. Furthermore, permutation tests calculated by 100 randomizations were performed to avoid the overfitting of supervised OPLS-DA models. The false detection rate (FDR)-corrected Mann-Whitney U tests was applied for the selection and validation of differential variables. The variable importance in projection (VIP) values of all peaks from the OPLS-DA model was taken as a coefficient for peak selection. The metabolites with statistical significance in both multivariate and univariate analyses (VIP > 1, pFDR < 0.05 and FC < 0.8 or > 1.2) were identified. The metabolic pathway analysis was conducted in the specialized online software MetaboAnalyst 5.0 [16].

2.8. RT-PCR

RNA was reverse transcribed to cDNA using RevertAid First Strand cDNA Synthesis Kit (Thermo Fisher, USA). Levels of mRNA expression were determined by RT-PCR with FastStart Universal SYBR Green Master (Roche, CH) on Real-Time PCR System (Stepone plus, ABI). The primer sequences were shown in supplementary file (Table S1). The expression levels of mRNA were normalized to GAPDH. Relative level of gene expression was calculated using the $2^{-\triangle\triangle Ct}$ method.

2.9. Statistical analysis

Data, expressed as means ± SD, was analyzed by using SPSS25.0 Software (IBM, USA). The differences between groups were examined by Student's t-test. $P < 0.05$ was considered to be statistically significant.

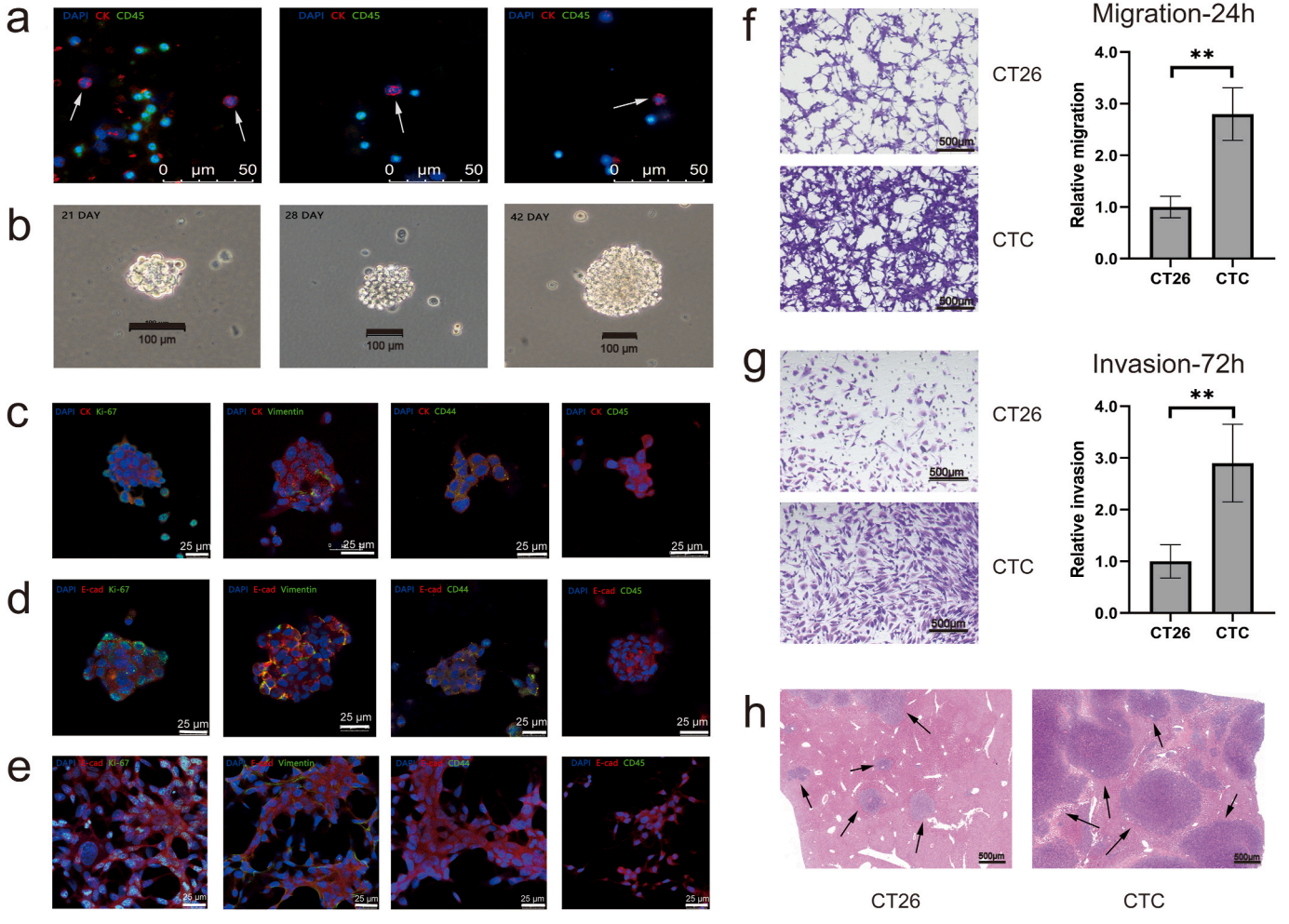

Figure 2. (a) Immunofluorescence staining showed positive expression of CTCs captured from colorectal cancer mice (white arrow). (b) Images of spheroids derived from isolated CTCs in different days. (c) Immunofluorescence staining showed CTC spheroids formed in vitro for 21 days. (d) Immunofluorescence staining showed CTC spheroids formed in vitro for 42 days. (e) Immunofluorescence staining showed single CTCs formed in vitro. (f) The migration and invasion ability of CTCs was detected by Transwell cell migration assays (**P < 0.01). (g) The invasion ability of CTCs was detected by Transwell cell invasion assays (**P < 0.01). (h) H & E section staining of a liver metastasis (black arrow).

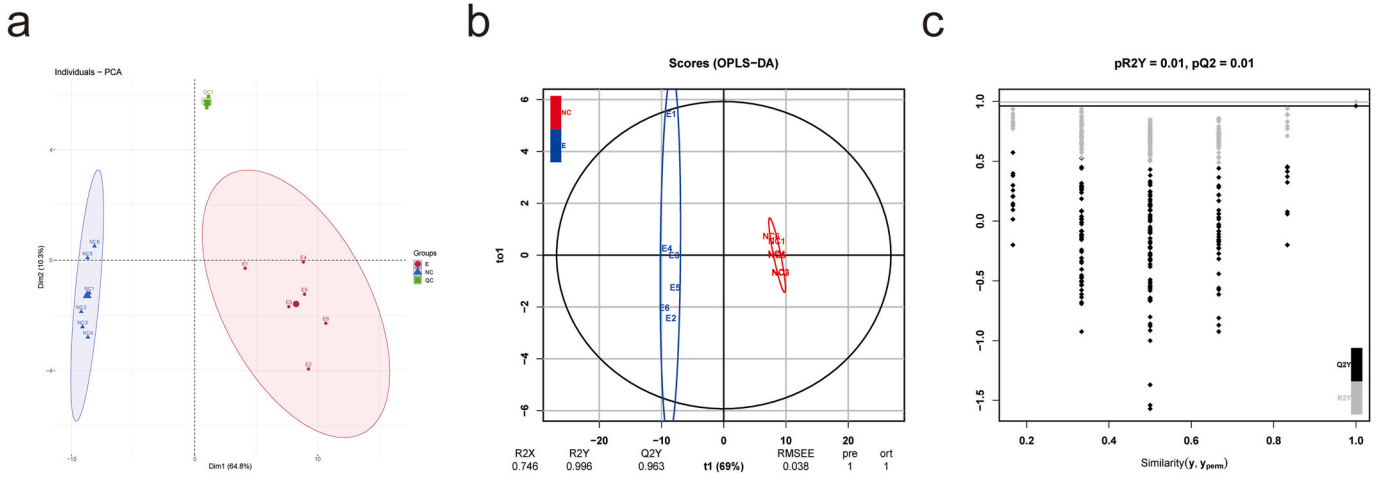

Figure 3. (a) Principal component score plot showing the homogeneity and group NC and group E. (b) Partial least squares discriminant analysis (PLS-DA) plot with sample identification, showing the discrimination between group NC and group E. (c) Validation plots of PLS-DA valid.

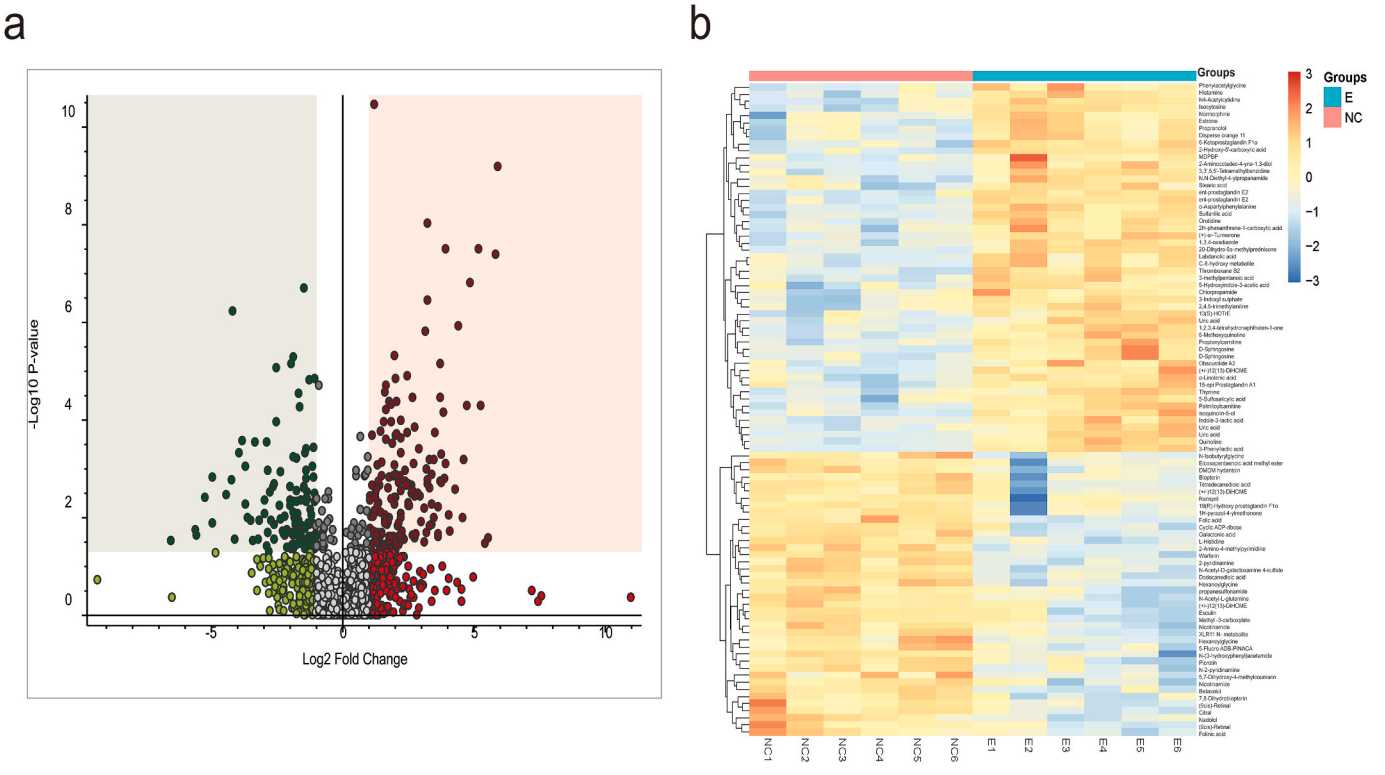

Figure 4. (a) Volcano plot analysis of the differential metabolic pathways between group NC and group E. (b) Heat map of differential metabolites from individual pairwise comparisons between group NC and group E.

3. Result

3.1. Enrichment and in-vitro culture of CTC from CRC mice

CTCs from CRC mice were negatively selected applying CD45 microbeads and magnetic rack to retain a wider CTCs group. Representative images of immunofluorescent stained CTCs mixed with white blood cells (WBCs) show CTCs identified as DAPI+/CD45−/CK+(Figure 2a). In CRC mice with detectable CTC (n = 12), the average count of CTCs in each 0.1 ml blood sample was 18 ± 11. Then, the enriched CTCs were transferred to the non-adherent plates in McCoy's 5A medium. Detectable CTC spheres formed after 21 days in culture, and started to proliferate steadily (Figure 2b). Moreover, immunocytochemistry experiments were performed with anti-CK, anti-CD45, anti-Ki-67, anti-CD44, anti- E-cad and anti-Vimentin antibodies, showing that CTC spheres were of epithelial origin and have undergone EMT process. At the same time, EMT generates CTC spheres with stem cell properties (Figure 2c). The culture was maintained for 42 days and shows an enhanced EMT phenotypes over time (Figure 2d). We found that the transfer of CTC spheres to the adherent plate may contribute to loss of stem cell properties (Figure 2e).

3.2. CTC exhibited increased migratory and invasive abilities

To investigate metastatic capacities of CTC, we executed Transwell assays upon the seeded 1×10^4 cells. The outcomes showed that more migrated CTCs were detected after incubation. CTCs exhibit 2.8-fold higher tendency of migration than the CT26 cells (Figure 2f). The invasion abilities of CTCs are markedly enhanced after 72 h (Figure 2g). we further investigated the ability of tumorigenesis upon CTCs in-vivo. CTCs and CT26 cells were injected into the spleen of the BALB/c nude mice respectively. Pathological sections of liver show that CTCs induced more metastasis foci in the liver than that by the CT26 cells (Figure 2h). These experimental results indicated the apparently increased invasive ability of CTCs.

3.3. HPLC-MS based untargeted metabolomics

Liver metastasis tissue samples were analyzed by using an untargeted HPLC-MS based metabolomics analysis, including liver metastasis tissues from the CT26 cells derived mouse models (group NC, n = 6) and liver metastasis tissues from the CTC derived mouse models (group E, n = 6). OPLS-DA and PCA were directed to detect the distinctions between the group E and group NC. The PCA score scatter plots show a separation tendency between the group E and group NC liver metastasis tissues, which indicate significant differences in the levels of metabolites between two groups (Figure 3a). The OPLS-DA method is a supervised discriminant analysis statistical method, therefore, could produce a better separation between classification groups. The OPLS-DA score parameters that are showed to R2Y = 0.996, Q2Y = 0.963 (Figure 3b). The cross-validation algorithm shows high R2, high Q2 values and a high accuracy (Figure 3c). These data pointed out the prevailing predictability and the highly effective validation of this model.

3.4. Differential metabolites analysis and enrichment analysis

The acquired data from HPLC-MS analysis were sorted out by CD2.1 and identified metabolites were realized by the database

Table 1
List of metabolites significantly changed in liver metastasis tissues from the CTC derived mouse models (group E, n = 6) compared to the CT26 cells derived mouse models (group NC, n = 6), paired Welch's t test.

Metabolites	Molecular Weight	Fold change	Retention time (min)	Direction of change in metastasis	p value
L-Histidine	155.0694	1.83	27.72	↑	3.25E-02
Niacinamide	122.0482	2.48	1.49	↑	3.90E-02
Folic acid	441.1396	3.27	9.87	↑	3.25E-02
9-cis-Retinal	284.2136	3.18	22.04	↑	3.90E-02
Prostaglandin F1a	372.2507	2.49	15.656	↑	3.25E-02
5-Formyltetrahydrofolic acid	473.1659	8.04	9.571	↑	3.90E-02
Isobutyrylglycine	145.0727	4.17	6.001	↑	3.90E-02
5-Fluorouridine	362.2088	2.61	14.263	↑	3.90E-02
Biopterin	237.0862	2.03	4.071	↑	3.25E-02
N-Acetyl glutamine	188.0787	2.69	2.396	↑	3.25E-02
7,8-Dihydrobiopterin	239.1018	2.07	4.075	↑	3.90E-02
Cyclic ADP-ribose	541.0610	1.91	4.475	↑	3.90E-02
12,13-DHOME	296.2348	0.36	19.92	↓	3.25E-02
Sphingosine	281.2713	0.34	16.8	↓	3.25E-02
Uric acid	151.0017	0.10	3.06	↓	3.90E-02
L-Palmitoyl carnitine	399.3340	0.12	17.83	↓	3.25E-02
13-HETE	294.2192	0.27	19.72	↓	3.90E-02
Thromboxane B2	392.2168	0.33	16.03	↓	3.25E-02
Alpha-Linolenic acid	278.2242	0.32	19.763	↓	3.25E-02
5-Hydroxyindoleacetic acid	191.0580	0.34	10.736	↓	3.90E-02
Aspartyl phenylalanine	280.1058	0.24	7.54	↓	3.25E-02

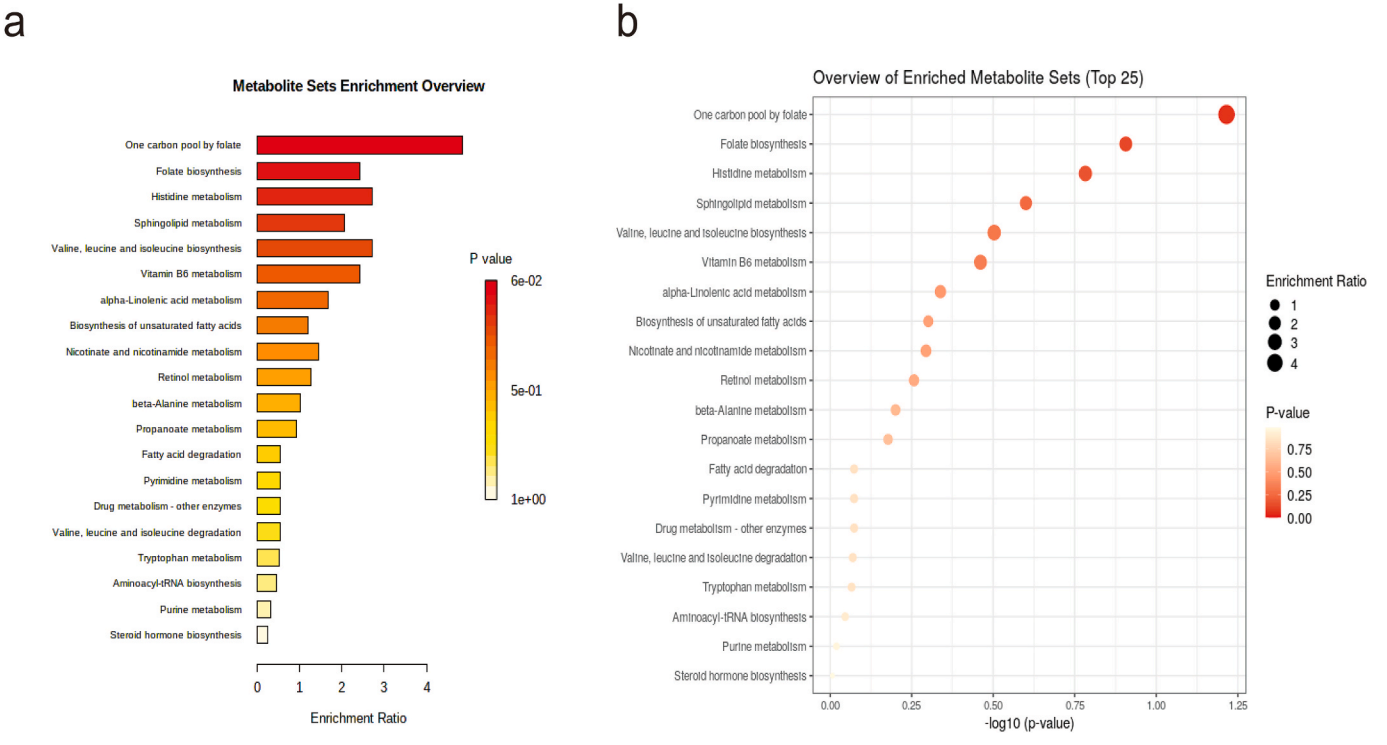

Figure 5. (a) Bar graphs of the differential metabolic pathways. (b) General overview of the enriched metabolite class sets.

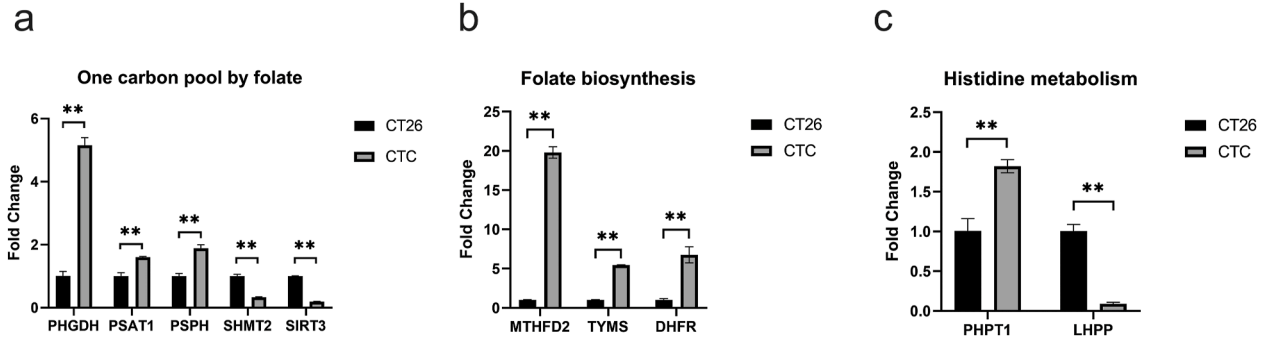

Figure 6. RT-PCR was used to detect the mRNA expression of energy metabolism-related genes in liver metastases. (*p < 0.05, **p < 0.01, t test). (a) enzymes involved in one carbon pool by folate (PHGDG, PSAT1, PSPH, SHMT2, SIRT3). (b) enzymes involved in folate biosynthesis(MTHFD2, TYMS, DHFR). (c) enzymes involved in histidine metabolism (PHPT1, LHPP).

(mzCloud, mzVault). Only compounds with a high mzCloud match (>80) were assigned an identity and used in subsequent analyses. In the univariate analysis, including volcano plot analysis (Figure 4a) and heat map (Figure 4b), we screened 288 differential metabolites, of which 119 metabolites are downregulated and 169 metabolites are upregulated significantly (VIP > 1, pFDR < 0.05 and FC < 0.8 or > 1.2). Table 1 shows some of the metabolites that have changed significantly. To further investigate the alterations in metabolic pathway, pathway enrichment analysis was conducted using MetaboAnalyst 5.0 [16]. The corresponding metabolic pathways are exhibited in Figure 5a and b, including one carbon pool by folate, folate biosynthesis, histidine metabolism, sphingolipid metabolism, vitamin B6 metabolism, alpha-Linolenic acid metabolism, biosynthesis of unsaturated fatty acids, nicotinate and nicotinamide metabolism, and retinol metabolism, *etc*.

3.5. Expression analysis of genes involved in key metabolic pathways

To correlate the metabolomics data with gene expression, we performed RT-PCR analyses on the same samples. RT-PCR analyses confirmed a tendency in gene expression changes that were uniform with our metabolomics data and shown a specific up-regulation of mRNAs involved in one carbon pool by folate (Figure 6a), folate biosynthesis (Figure 6b), and histidine metabolism (Figure 6c) in the liver metastasis of the CTC derived mouse models ($P < 0.05$). The up-regulated genes included the phosphoglycerate dehydrogenase (PHGDH), phosphoserine aminotransferase 1 (PSAT1) and phosphoserine phosphatase (PSPH) which involved in one carbon pool by folate. Also, key enzymes were up-regulated in the folate biosynthesis, methylenetetrahydrofolate dehydrogenase 2 (MTHFD2), thymidylate synthetase (TYMS) and dihydrofolate reductase (DHFR). Phosphohistidine phosphatase 1 (PHPT1) in histidine metabolism was up-regulated as well.

4. Discussion

CTCs are a subset of tumor cells that shed from the primary tumor and metastasis site, and intravasation into the circulation is a precondition for spreading to remote organ to form metastasis in certain tumor entities [8, 17]. Tumor cells can depart from the primary organ at different stages of tumor progression and develop independently at the metastatic site [18]. EMT implicates the transition of CTCs through multiple phenotypic states, including the acquisition of stem cell characteristics and the enhancement of migration and invasion capabilities [19, 20]. In our present study, the CTCs isolated and enriched from the peripheral blood of colorectal cancer-bearing mice could generate an established stable CTC line. Besides its capacity to proliferate steadily, it exhibits a mixed epithelial and mesenchymal phenotype with stem cell–like properties. Furthermore, Transwell assays and liver metastasis model confirmed that CTCs possess stronger migration and invasion abilities than the parental CT26 cells. Our strategy of constructing the CTC-derived mice xenograft for investigation of the metabolic feature of CTCs derived metastases is more facile and accessible than that using ex vivo culture of the isolated CTC from the patient-derived xenograft (PDX) mice models of the non-small cell lung cancer (NSCLC) patients [21] and breast cancer patients [14]. However, it hardly provides comprehensive omics molecular characteristics of the cancer metastasis from specific cancer patients.

A series of complex factors, including the gene mutations and microenvironmental remodeling throughout tumor progression and malignant transformation, may lead to metabolic modifications in CTCs [15, 22]. In this study, we used a LC-MS metabolomic platform to analyze the metabolic differences between the tumor cells that have metastasized to liver. Paired analysis of CTCs and parental CT26 cells for liver metastases disclosed a quantity of considerably changed metabolites between the tissues. The differential metabolites identified by mzCloud, which are involved in the one carbon pool by folate, folate biosynthesis, histidine metabolism.

DNA methylation and nucleotide synthesis are the biochemical foundations of cancers extremely dependent on one-carbon unit. Tumor cells increased the supply of one-carbon units to maintain rapid proliferation by rapidly ingesting exogenous serine. When exogenous serine is lacking, the tumor cells can activate the serine synthesis pathway (SSP) to produce serine [23, 24]. PHGDH, PSAT1 and PSPH are three key enzymes in SSP, and their elevated expression was observed in a variety of tumors [25]. In the present study, comparison of CTCs and parental CT26 cells in liver metastases also revealed that PHGDH, PSAT1 and PSPH are up-regulated in CTCs derived liver metastases. Therefore, CTCs have up-regulated SSP to obtain more one-carbon units, enhancing their ability to migrate and invade, and thereby supporting hematogenous dissemination of CTCs to liver.

Folate biosynthesis plays a crucial role in transporting one-carbon units. One-carbon units cannot exist in a free form, and is usually combined with tetrahydrofolate (THF) to participate in biological metabolism [26]. If THF is reduced, the cells hardly get sufficient one carbon unit, which will inhibit the growth and aggressiveness of tumor cells [27]. DHFR is a key enzyme responsible for intracellular folate biosynthesis, which is essential for tumor treatment [28]. MTHFD2 continues to be highly expressed in patients with various kinds of cancer types, and high expression of MTHFD2 is accompanied by an unfavorable prognosis. Knockdown of MTHFD can lead to a decrease in the ratio of NADPH/NADP+ and GSH/GSSG in cells, thereby increasing the sensitivity of tumor cells to ROS [29]. The High expression of TYMS reportedly contributes to low survival and acquired resistance to combined chemotherapy in CRC patients [30]. Moreover, our study indicates that the expression of DHFR, MTHFD2 and TYMS are up-regulated in CTCs liver metastases. In order to maintain rapid proliferation, CTCs displayed a high level of oxidative stress; meanwhile, CTCs elevate the expression of MTHFD2 in folate biosynthesis to scavenge the intracellular ROS. In addition, the mutation also renders CTCs particularly resistant to traditional chemotherapy.

Histidine metabolism plays an important role in tumor migration, invasion, and poor prognosis. In a recent study, the authors found that PHPT1 may be related to the reorganization of the actin cytoskeleton, thereby affecting the migration and invasion of lung cancer cells [31]. In this study, the elevated expression of PHPT1 in CTCs derived liver metastasis tissues has been observed, which may be related to the high migration and invasion of CTCs.

To conclude, our research provides novel perceptions into the metabolism profiling of the liver metastasis stemmed from CTCs obtained in peripheral blood of CRC tumor mice. LC-MS possesses high sensitivity and high unit mass accuracy to identify a number of metabolites. However, given its continuous nature, conventional LC-MS rarely achieves 100% duty cycle, resulting in that more quantity of samples is required [32]. The CTC cultured *in vitro* is often difficult or costly, and as such, is a considerable limitation of CTC studies. Owning to a restricted sample size, the results ought to be further confirmed in future research. Chemical isotope labeling nano LC-MS method has great potential for high-coverage quantitative metabolomics of 100–10,000 cells [33]. The difference of metabolic reprogramming features may be related to heterogeneity across cell types. To circumvent discrepancies between model systems, we are also trying to establish a stable CTC line from the CRC patients.

Declarations

Author contribution statement

Meng Li: Conceived and designed the experiments; Performed the experiments; Analyzed and interpreted the data; Wrote the paper.

Shengming Wu: Performed the experiments; Contributed reagents, materials, analysis tools or data.

Chengle Zhuang; Chenzhang Shi; Lei Gu: Analyzed and interpreted the data.

Peng Wang: Performed the experiments.

Fangfang Guo: Contributed reagents, materials, analysis tools or data.

Yilong Wang; Zhongchen Liu: Conceived and designed the experiments; Wrote the paper.

Funding statement

This work was supported by the National Natural Science Foundation of China [grant numbers 32071395, 32271439, 82070533]; the intramural research program of Shanghai Tenth People's Hospital affiliated Tongji University [grant number 2021SYPDRC013]; and the Fundamental Research Funds for the Central Universities.

Data availability statement

Data will be made available on request.

Declaration of interest's statement

The authors declare no competing interests.

Additional information

Supplementary content related to this article has been published online at https://doi.org/10.1016/j.heliyon.2022.e12515.

References

[1] H. Sung, J. Ferlay, R.L. Siegel, M. Laversanne, I. Soerjomataram, A. Jemal, F. Bray, Global cancer statistics 2020: GLOBOCAN estimates of incidence and mortality worldwide for 36 cancers in 185 countries, CA A Cancer J. Clin. 71 (2021) 209–249.

[2] J.W. Lee, M.L. Stone, P.M. Porrett, S.K. Thomas, C.A. Komar, J.H. Li, D. Delman, K. Graham, W.L. Gladney, X. Hua, T.A. Black, A.L. Chien, K.S. Majmundar, J. C. Thompson, S.S. Yee, M.H. O'Hara, C. Aggarwal, D. Xin, A. Shaked, M. Gao, D. Liu, M.J. Borad, R.K. Ramanathan, E.L. Carpenter, A. Ji, M.C. de Beer, F.C. de Beer, N.R. Webb, G.L. Beatty, Hepatocytes direct the formation of a pro-metastatic niche in the liver, Nature 567 (2019) 249–252.

[3] Z. Wu, D. Wei, W. Gao, Y. Xu, Z. Hu, Z. Ma, C. Gao, X. Zhu, Q. Li, TPO-induced metabolic reprogramming drives liver metastasis of colorectal cancer CD110+ tumor-initiating cells, Cell Stem Cell 17 (2015) 47–59.

[4] J.M. Loo, A. Scherl, A. Nguyen, F.Y. Man, E. Weinberg, Z. Zeng, L. Saltz, P.B. Paty, S.F. Tavazoie, Extracellular metabolic energetics can promote cancer progression, Cell 160 (2015) 393–406.

[5] K. Pantel, M.R. Speicher, The biology of circulating tumor cells, Oncogene 35 (2016) 1216–1224.

[6] J. Chen, C. Ye, J. Dong, S. Cao, Y. Hu, B. Situ, X. Xi, S. Qin, J. Xu, Z. Cai, L. Zheng, Q. Wang, Metabolic classification of circulating tumor cells as a biomarker for metastasis and prognosis in breast cancer, J. Transl. Med. 18 (2020) 59.

[7] D. Yang, X. Yang, Y. Li, P. Zhao, R. Fu, T. Ren, P. Hu, Y. Wu, H. Yang, N. Guo, Clinical significance of circulating tumor cells and metabolic signatures in lung cancer after surgical removal, J. Transl. Med. 18 (2020) 243.

[8] Y. Abouleila, K. Onidani, A. Ali, H. Shoji, T. Kawai, C.T. Lim, V. Kumar, S. Okaya, K. Kato, E. Hiyama, T. Yanagida, T. Masujima, Y. Shimizu, K. Honda, Live single cell mass spectrometry reveals cancer-specific metabolic profiles of circulating tumor cells, Cancer Sci. 110 (2019) 697–706.

[9] I. Baccelli, A. Schneeweiss, S. Riethdorf, A. Stenzinger, A. Schillert, V. Vogel, C. Klein, M. Saini, T. Bauerle, M. Wallwiener, T. Holland-Letz, T. Hofner, M. Sprick, M. Scharpff, F. Marme, H.P. Sinn, K. Pantel, W. Weichert, A. Trumpp, Identification of a population of blood circulating tumor cells from breast cancer patients that initiates metastasis in a xenograft assay, Nat. Biotechnol. 31 (2013) 539–544.

[10] C. Agnoletto, F. Corra, L. Minotti, F. Baldassari, F. Crudele, W.J.J. Cook, G. Di Leva, A.P. d'Adamo, P. Gasparini, S. Volinia, Heterogeneity in circulating tumor cells: the relevance of the stem-cell subset, Cancers(Basel) 11 (2019).

[11] T.S. Gujral, M. Chan, L. Peshkin, P.K. Sorger, M.W. Kirschner, G. MacBeath, A noncanonical Frizzled2 pathway regulates epithelial-mesenchymal transition and metastasis, Cell 159 (2014) 844–856.

[12] V. Padmanaban, I. Krol, Y. Suhail, B.M. Szczerba, N. Aceto, J.S. Bader, A.J. Ewald, E-cadherin is required for metastasis in multiple models of breast cancer, Nature 573 (2019) 439–444.
[13] M. Maeshiro, S. Shinriki, R. Liu, Y. Nakachi, Y. Komohara, Y. Fujiwara, K. Ohtsubo, R. Yoshida, K. Iwamoto, H. Nakayama, H. Matsui, Colonization of distant organs by tumor cells generating circulating homotypic clusters adaptive to fluid shear stress, Sci. Rep. 11 (2021) 6150.
[14] B.M. Szczerba, F. Castro-Giner, M. Vetter, I. Krol, S. Gkountela, J. Landin, M.C. Scheidmann, C. Donato, R. Scherrer, J. Singer, C. Beisel, C. Kurzeder, V. Heinzelmann-Schwarz, C. Rochlitz, W.P. Weber, N. Beerenwinkel, N. Aceto, Neutrophils escort circulating tumour cells to enable cell cycle progression, Nature 566 (2019) 553–557.
[15] S. Gkountela, F. Castro-Giner, B.M. Szczerba, M. Vetter, J. Landin, R. Scherrer, I. Krol, M.C. Scheidmann, C. Beisel, C.U. Stirnimann, C. Kurzeder, V. Heinzelmann-Schwarz, C. Rochlitz, W.P. Weber, N. Aceto, Circulating tumor cell clustering shapes DNA methylation to enable metastasis seeding, Cell 176 (2019) 98–112 e114.
[16] Z. Pang, J. Chong, G. Zhou, D.A. de Lima Morais, L. Chang, M. Barrette, C. Gauthier, P.E. Jacques, S. Li, J. Xia, MetaboAnalyst 5.0: narrowing the gap between raw spectra and functional insights, Nucleic Acids Res. 49 (2021) W388–W396.
[17] N. Malara, V. Trunzo, U. Foresta, N. Amodio, S. De Vitis, L. Roveda, M. Fava, M. Coluccio, R. Macri, A. Di Vito, N. Costa, C. Mignogna, D. Britti, E. Palma, V. Mollace, Ex-vivo characterization of circulating colon cancer cells distinguished in stem and differentiated subset provides useful biomarker for personalized metastatic risk assessment, J. Transl. Med. 14 (2016) 133.
[18] P. Eliasova, M. Pinkas, K. Kolostova, R. Gurlich, V. Bobek, Circulating tumor cells in different stages of colorectal cancer, Folia Histochem. Cytobiol. 55 (2017) 1–5.
[19] V. Devaraj, B. Bose, Morphological state transition dynamics in EGF-induced epithelial to mesenchymal transition, J. Clin. Med. 8 (2019).
[20] W. Guo, Z. Keckesova, J.L. Donaher, T. Shibue, V. Tischler, F. Reinhardt, S. Itzkovitz, A. Noske, U. Zurrer-Hardi, G. Bell, W.L. Tam, S.A. Mani, A. van Oudenaarden, R.A. Weinberg, Slug and Sox9 cooperatively determine the mammary stem cell state, Cell 148 (2012) 1015–1028.
[21] K.N. Suvilesh, Y. Manjunath, V. Radhakrishnan, D.M. Avella, E.T. Kimchi, K.F. Staveley-O'Carroll, G. Li, J.T. Kaifi, Abstract LB-271: multi-omics characterization of tumor tissues from CTC derived xenograft (CDX) mouse models of early-stage NSCLC patients reveals novel diagnostic/therapeutic target(s), Cancer Res. 80 (2020). LB-271-LB-271.
[22] C. Donato, L. Kunz, F. Castro-Giner, A. Paasinen-Sohns, K. Strittmatter, B.M. Szczerba, R. Scherrer, N. Di Maggio, W. Heusermann, O. Biehlmaier, C. Beisel, M. Vetter, C. Rochlitz, W.P. Weber, A. Banfi, T. Schroeder, N. Aceto, Hypoxia triggers the intravasation of clustered circulating tumor cells, Cell Rep. 32 (2020), 108105.
[23] O.D. Maddocks, C.R. Berkers, S.M. Mason, L. Zheng, K. Blyth, E. Gottlieb, K.H. Vousden, Serine starvation induces stress and p53-dependent metabolic remodelling in cancer cells, Nature 493 (2013) 542–546.
[24] A.C. Newman, O.D.K. Maddocks, Serine and functional metabolites in cancer, Trends Cell Biol. 27 (2017) 645–657.
[25] S. Pollari, S.M. Kakonen, H. Edgren, M. Wolf, P. Kohonen, H. Sara, T. Guise, M. Nees, O. Kallioniemi, Enhanced serine production by bone metastatic breast cancer cells stimulates osteoclastogenesis, Breast Cancer Res. Treat. 125 (2011) 421–430.
[26] H.B. Yang, Y.Y. Xu, X.N. Zhao, S.W. Zou, Y. Zhang, M. Zhang, J.T. Li, F. Ren, L.Y. Wang, Q.Y. Lei, Acetylation of MAT IIalpha represses tumour cell growth and is decreased in human hepatocellular cancer, Nat. Commun. 6 (2015) 6973.
[27] A.C. Newman, O.D.K. Maddocks, One-carbon metabolism in cancer, Br. J. Cancer 116 (2017) 1499–1504.
[28] M.A. Fawal, T. Jungas, A. Davy, Inhibition of DHFR targets the self-renewing potential of brain tumor initiating cells, Cancer Lett. 503 (2021) 129–137.
[29] H.Q. Ju, Y.X. Lu, D.L. Chen, Z.X. Zuo, Z.X. Liu, Q.N. Wu, H.Y. Mo, Z.X. Wang, D.S. Wang, H.Y. Pu, Z.L. Zeng, B. Li, D. Xie, P. Huang, M.C. Hung, P.J. Chiao, R. H. Xu, Modulation of redox homeostasis by inhibition of MTHFD2 in colorectal cancer: mechanisms and therapeutic implications, J. Natl. Cancer Inst. 111 (2019) 584–596.
[30] Z. Wang, J.Q. Chen, J.L. Liu, X.G. Qin, Y. Huang, Polymorphisms in ERCC1, GSTs, TS and MTHFR predict clinical outcomes of gastric cancer patients treated with platinum/5-Fu-based chemotherapy: a systematic review, BMC Gastroenterol. 12 (2012) 137.
[31] S.C. Kwon, T.A. Nguyen, Y.G. Choi, M.H. Jo, S. Hohng, V.N. Kim, J.S. Woo, Structure of human DROSHA, Cell 164 (2016) 81–90.
[32] Y. Li, M. Bouza, C. Wu, H. Guo, D. Huang, G. Doron, J.S. Temenoff, A.A. Stecenko, Z.L. Wang, F.M. Fernández, Sub-nanoliter metabolomics via mass spectrometry to characterize volume-limited samples, Nat. Commun. 11 (1) (2020 Nov 6) 5625.
[33] X. Luo, L. Li, Metabolomics of small numbers of cells: metabolomic profiling of 100, 1000, and 10000 human breast cancer cells, Anal. Chem. 89 (21) (2017) 11664–11671.